Optical Signal Processing: Data Exchange

Jian Wang and Alan E. Willner

Additional information is available at the end of the chapter

http://dx.doi.org/10.5772/52205

1. Introduction

Optical signal processing is considered to be an attractive technique to enable fast signal manipulation in the optical domain which can avoid cumbersome optical-electrical-optical (OEO) conversions [1]. Driven by the rapid increase of traffic rates, network capacity and complexity, advanced optical networks raise the significance of data traffic grooming and require different optical signal processing functions at network nodes to achieve enhanced network efficiency and flexibility. Typical optical signal processing operations include wavelength conversion, logic gate, format conversion, delay for buffer, regeneration, add/drop, (de)multiplexing, multicasting, etc [2-14]. One may note that most of these functions work in a similar fashion of unidirectional information transfer. For example, wavelength conversion copies information from one wavelength and transfers it onto another wavelength [2]. To achieve superior network performance, bidirectional information swapping, named data exchange, would be expected to provide enhanced flexibility of optical signal processing compared to unidirectional information transfer [15].

Generally speaking, as an important concept for efficiently utilizing network resources and improving network performance, data exchange refers to the information swapping between different wavelengths/time-slots/polarizations or other degrees of freedom. In the wavelength domain (e.g., wavelength-division multiplexed (WDM) network), data exchange, which is also known as wavelength exchange or wavelength interchange, would require the swapping of data from one wavelength with the data from another wavelength. Extensions of data exchange would expect the data swapping between different time-slots in the time domain (e.g., optical time-division multiplexed (OTDM) network), different polarization states in the polarization domain (e.g., polarization-multiplexed (pol-muxed) network), and different "twisted" light beams carrying different orbital angular momentum (OAM) values in the phase front domain (e.g., OAM-multiplexed network). Moreover, the recently increasing interest of ad-

vanced modulation formats [16, 17] would require the data exchange to be available for different modulation formats, such as on-off keying (OOK), differential phase-shift keying (DPSK), differential quadrature phase-shift keying (DQPSK), pol-muxed, etc.

The emergence of nonlinear optics has triggered increased interest and paved a potential way to develop optical signal processing in high-speed optical networks [18, 19]. Optical nonlinearities (e.g. $\chi^{(2)}$ and $\chi^{(3)}$), including difference-frequency generation (DFG) [20, 21], cascaded sum- and difference-frequency generation (cSFG/DFG) [22-26], degenerate/non-degenerate four-wave mixing (FWM) [27-47], and Kerr-induced nonlinear polarization rotation [48-50], are potentially suitable candidates to enable data exchange. In some cases, simple linear optics may also provide an alternative approach to facilitating data exchange [51, 52]. To fulfill the rapid development of high-speed large-capacity optical communications with emerging multiplexing/demultiplexing techniques and advanced modulation formats, as shown in Fig. 1, a laudable goal would be to achieve robust data exchange in different degrees of freedom (wavelength, time, polarization, phase front), for different modulation formats (OOK, DPSK, DQPSK, pol-muxed), and at different granularities (entire data, groups of bits, tributary channels).
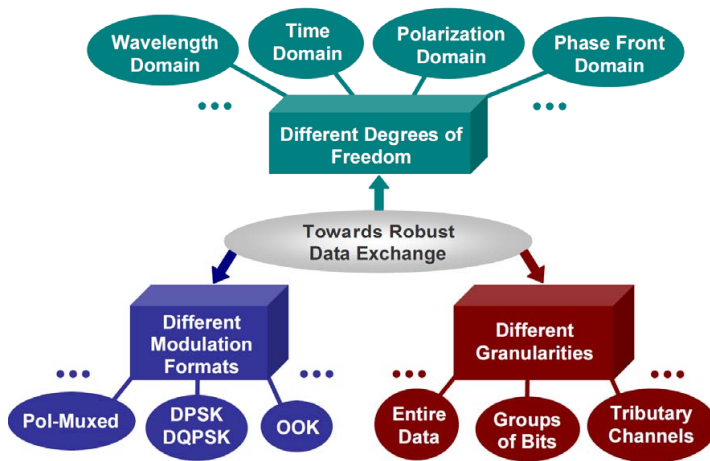

Figure 1. Schematic illustration of robust data exchange.

In this chapter, we tend to provide a comprehensive review of research works towards robust data exchange using various optical nonlinearities [22-50, 53] and simple linear optics [51, 52]. Several kinds of optical nonlinearities are employed: (1) cSFG/DFG in a periodically poled lithium niobate (PPLN) waveguide; (2) non-degenerate FWM in a highly nonlinear fiber (HNLF); (3) bidirectional degenerate FWM in an HNLF; (4) Kerr-induced nonlinear polarization rotation in an HNLF; (5) Conversion-dispersion-based tunable delays. We start with a conceptual description of data exchange followed by state-of-the-art results.

2. Concept of data exchange

Robust data exchange in the wavelength, time, polarization and phase front domains might be valuable for superior network performance. As an example, a desirable goal of data exchange would be to efficiently utilize nonlinearities in the wavelength domain, such that the data between two different wavelengths can be "exchanged", i.e., swapped, using nonlinear processes in a single device [54]. Figure 2(a) illustrates the basic concept of data exchange in the wavelength domain (wavelength exchange/interchange), which is a wavelength-domain data manipulation enabling the swapping of data between two different wavelengths. One straightforward way, as shown in Fig. 2 (b), is to use two separate wavelength converters (WCs) with one performing the wavelength conversion from signal A (Sig. A) to signal B (Sig. B), and the other from signal B to signal A. Towards single-device operation, one simple way of data exchange in the wavelength domain is to explore the combined signal depletion and wavelength conversion effects in a nonlinear device including a piece of HNLF or a PPLN waveguide [55-58]. Non-degenerate FWM ($\chi^{(3)}$) in an HNLF [29-45] and cascaded second-order nonlinearities ($\chi^{(2)} : \chi^{(2)}$) in a PPLN waveguide [22-26] are potential choices to realize such data exchange. As shown in Fig. 2 (c), due to the signal depletion and wavelength conversion effects, the data carried by signal A is consumed and converted to the wavelength of signal B and vice versa. This enables single-device-based data exchange in the wavelength domain. Similar concepts of data exchange in the time, polarization and phase front domains are also available enabled by various optical nonlinearities or linear optics.
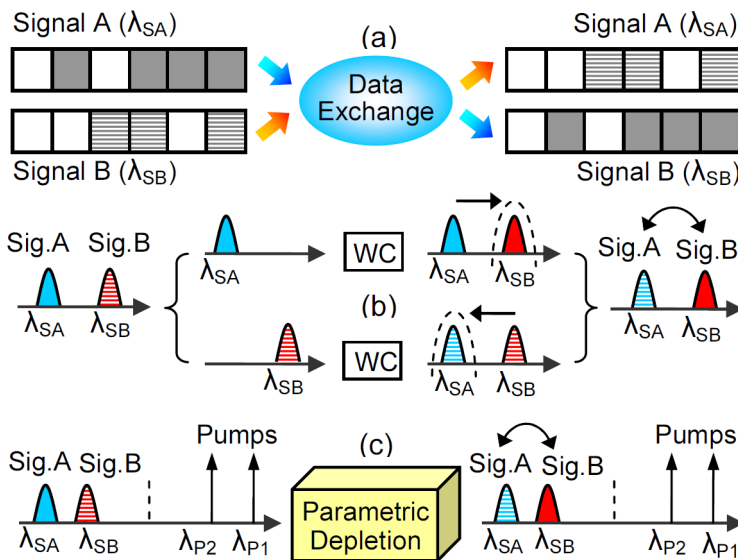

Figure 2. (a) Concept of data exchange in the wavelength domain. (b) Data exchange by two separate wavelength converters (WCs). (c) An example of data exchange by signal depletion and wavelength conversion in a single nonlinear device.

3. Recent advances for robust data exchange

3.1. Data exchange using cSFG/DFG in a single PPLN waveguide [22-26]

As depicted in Fig. 2(c), data exchange based on signal depletion and wavelength conversion of cSFG/DFG involves two signals and two pumps, which can be described by the coupled-mode equations. To better understand the single-PPLN-based data exchange, under the slowly varying amplitude approximation, we can derive the following analytical solutions to the complex amplitudes of signal A ($A_{SA}(L)$) and signal B ($A_{SB}(L)$) after data exchange [22]

$$A_{SA}(L) = A_{SA}(0) + \omega_{SA}\omega_{SF}\kappa_1\frac{1}{M^2}A_{P1}^*(0)[\kappa_1 A_{P1}(0)A_{SA}(0) + \kappa_2 A_{P2}(0)A_{SB}(0)][\cos(ML)-1] \quad \text{(a)}$$

$$A_{SB}(L) = A_{SB}(0) + \omega_{SB}\omega_{SF}\kappa_2\frac{1}{M^2}A_{P2}^*(0)[\kappa_1 A_{P1}(0)A_{SA}(0) + \kappa_2 A_{P2}(0)A_{SB}(0)][\cos(ML)-1] \quad \text{(b)}$$

$$(1)$$

where $M = \sqrt{\omega_{SA}\omega_{SF}\kappa_1^2 P_{P1}(0) + \omega_{SB}\omega_{SF}\kappa_2^2 P_{P2}(0)}$. $A_{SA}(0)$, $A_{SB}(0)$, $A_{P1}(0)$ and $A_{P2}(0)$ are the input complex amplitudes of signal A, signal B, pump 1 and pump 2, respectively. $P_{P1}(0)$ and $P_{P2}(0)$ are the input power of pump 1 and pump 2. κ_1 (κ_2) refers to the coupling coefficient of the second-order nonlinear interaction involving signal A (signal B) and pump 1 (pump 2). ω_{SA}, ω_{SB} and ω_{SF} are the angular frequencies of signal A, signal B and sum-frequency (SF) wave, respectively. L is the waveguide length.

When ignoring the initial pump phase and setting the same power for two input pumps, we can further simplify Eqs. (1a)(1b) as follows

$$A_{SA}(L) = \frac{\cos(ML)+1}{2}A_{SA}(0) + \frac{\cos(ML)-1}{2}A_{SB}(0) \quad \text{(a)}$$

$$A_{SB}(L) = \frac{\cos(ML)-1}{2}A_{SA}(0) + \frac{\cos(ML)+1}{2}A_{SB}(0) \quad \text{(b)}$$

$$(2)$$

When satisfying the following relationship written by

$$ML = (2N+1)\pi, \quad N = 0, 1, 2, 3 \cdots\cdots \quad\quad (3)$$

we can obtain

$$A_{SA}(L) = -A_{SB}(0) \quad \text{(a)}$$

$$A_{SB}(L) = -A_{SA}(0) \quad \text{(b)}$$

$$(4)$$

From Eq. (4) it can be clearly seen that data exchange between signal A and signal B is achieved under the exchange condition governed by Eq. (3). In particular, beyond the data exchange for OOK signal, the complex relationship in Eq. (4) also implies the modulation-format-transparency characteristic of PPLN-based data exchange.

Following the similar principle of PPLN-based data exchange using signal depletion and wavelength conversion of cSFG/DFG, we can further perform robust data exchange functions, including time- and channel-selective data exchange between WDM channels [23, 24] and low-speed tributary channel exchange of high-speed OTDM signals [25, 26].

The conceptual diagram of the proposed single-PPLN-based time- and channel-selective data exchange between WDM channels is illustrated in Fig. 3 [23, 24]. Multiple WDM channels (S1-S4) and two synchronized gated pumps (PA, PB) are coupled into a PPLN waveguide, in which cSFG/DFG processes take place. The wavelength selectivity of the quasi-phase matching (QPM) condition allows selection of channels for data exchange by proper choice of the two pump wavelengths. For proper QPM of both cSFG/DFG processes, the two pump wavelengths are nearly symmetric to the two exchanged data wavelengths with respect to the QPM wavelength. For instance, as illustrated in Fig. 3, within the gated pump pulse duration, PB mixes with S1 to produce an SF wave through the sum-frequency generation (SFG) process. Meanwhile, the SF wave interacts with PA to generate a new idler at the wavelength of S2 by the subsequent difference-frequency generation (DFG) process. During such nonlinear interactions, S1 can be depleted, and converted to S2 by means of proper control of the pump powers. Similarly, PA and S2 participate in the SFG process to create an SF wave, which simultaneously interacts with PB to yield an idler at the wavelength of S1 via the DFG process. Thus, S2 can also be consumed with its data copied onto S1. Consequently, it is expected to implement optical data exchange between S1 and S2 without the use of additional spectrum and touching other channels. Note that time- and channel-selective data exchange in specific time-slots (groups of bits) and between selective WDM channels can be accomplished by appropriately choosing the gated pump pulse duration and adjusting the pump wavelengths.
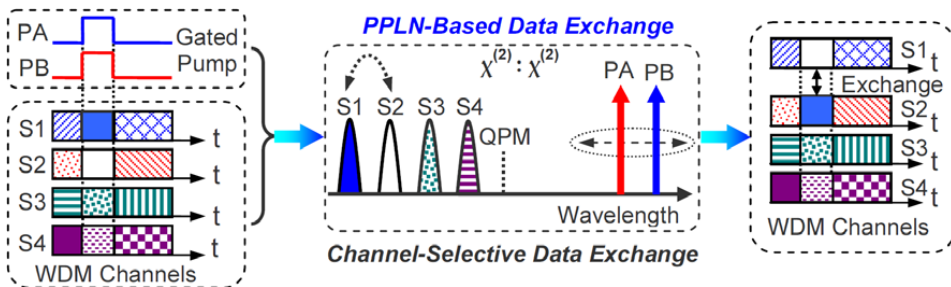

Figure 3. Concept and principle of single-PPLN-based time- and channel-selective data exchange between WDM channels.

We first demonstrate the data exchange between two 10-Gbit/s signals. Two gated pumps with a duty cycle of 1/127 and a pulse duration of ~3.2 ns are employed. The average power of each signal and peak power of each pump coupled into the PPLN waveguide are about 4 mW and 1 W, respectively. Figure 4 displays the observed temporal waveforms and eye diagrams of data exchange. The time-slots between the two straight lines correspond to the gated pump pulse duration, in which data exchange occurs. When S1

and the two pumps are on while S2 is off, the data of S1 within the gated pump pulse duration is depleted (a2) and converted to the wavelength of S2 (b3). Similarly, we can also observe the depletion of S2 (b2) and the conversion from S2 to S1 (a3) by switching S1 off and S2 on. In the case of simultaneously turning on the two signals and the two pumps, it is found that groups of bits data exchange between the two signals (S1 to S2: (b4), S2 to S1: (a4)) within the gated pump pulse duration is successfully achieved.
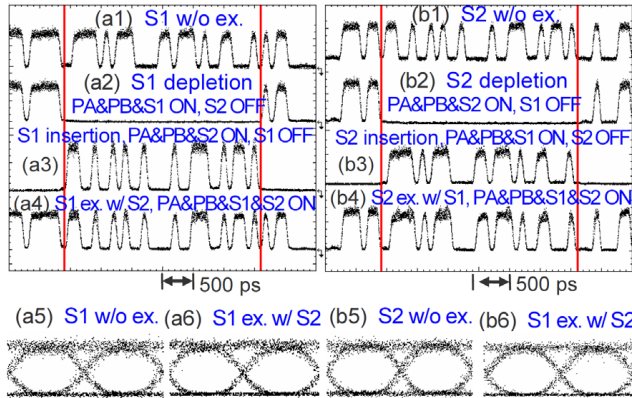
Figure 4. Measured (a1-a4)(b1-b4) temporal waveforms and (a5)(a6)(b5)(b6) eye diagrams of 10-Gbit/s groups of bits data exchange.

We further demonstrate the single-PPLN-based channel-selective data exchange for multiple WDM channels at 40 Gbit/s. Four WDM channels (S1: 1535.5 nm, S2: 1539.4 nm, S3: 1543.3 nm, S4: 1547.2 nm) are employed in the experiment. It is possible to perform a channel-selective data exchange by simply tuning the wavelength of the two pumps. Figure 5 displays the measured typical eye diagrams and bit-error rate (BER) performance for channel-selective data exchange between WDM channels. The power penalty of 40-Gbit/s channel-selective data exchange is estimated to be less than 4 dB at a BER of 10^{-9}.

Figure 6 illustrates the concept and principle of single-PPLN-based tributary channel exchange between two WDM high-speed OTDM signals [25, 26]. A PPLN waveguide is employed as the nonlinear device to perform the tributary channel exchange. Two WDM high-speed signals (S1, S2) each consisting of many low-speed time-division multiplexed tributary channels (e.g., 16 10-Gbit/s tributary channels for 160-Gbit/s signal), together with two synchronized subrate clock (e.g., 10 GHz) pumps, are launched into the PPLN waveguide for the tributary channel exchange. The wavelengths of two signals and two pumps are properly arranged to be symmetric (S1&P1, S2&P2) with respect to the QPM wavelength of PPLN. Inside the PPLN waveguide, two signals and two pumps participate in the cSFG/DFG nonlinear interactions, in which the photons of S1 (S2) and P1 (P2) are annihilated to produce the photons of SF wave, which are simultaneously consumed to generate the photons of S2 (S1) and P2 (P1). Due to the signal depletion and wavelength conversion ef-

fects, with the proper adjustment of pump powers, S1 can be depleted and converted to S2. Similarly, S2 can be extinguished to generate S1. As a result, data exchange between two signals (S1, S2) can be implemented. In particular, by exploiting two synchronized subrate (e.g., 10 GHz) clock pumps which are time aligned to one of the tributary channels of two WDM high-speed OTDM signals (e.g., 160 Gbit/s), it is possible to achieve the tributary channel exchange (e.g., 10 Gbit/s) between two WDM high-speed OTDM signals (e.g., 160 Gbit/s). As an example shown in Fig. 6, the tributary channel i (Ch. i) of two WDM high-speed OTDM signals is exchanged by using the signal depletion and wavelength conversion effects of cSFG/DFG in a PPLN waveguide.
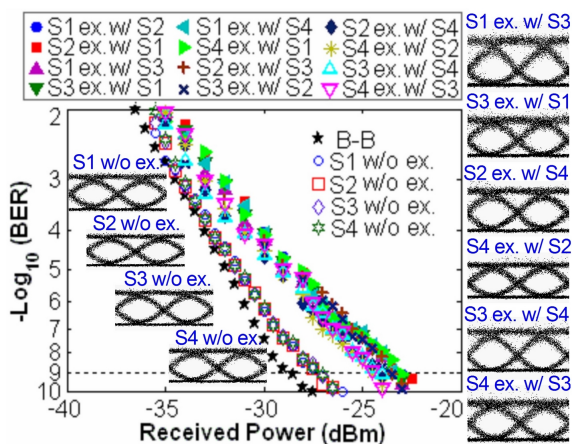

Figure 5. Measured eye diagrams and BER performance of 40-Gbit/s time- (groups of bits) and channel-selective data exchange between four WDM channels.
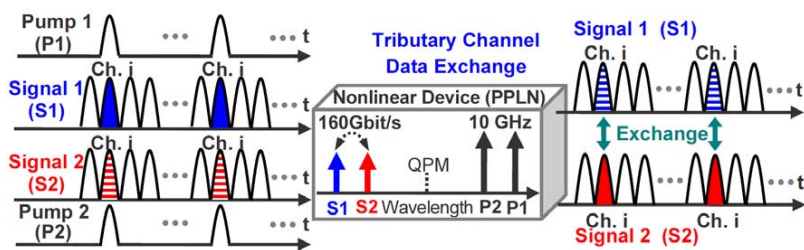

Figure 6. Concept and principle of single-PPLN-based tributary channel exchange between two WDM high-speed OTDM signals.

Figure 7 displays the eye diagrams for tributary channel exchange (Ch.1) measured by an optical sampling scope. Two 10-GHz clock pumps are time aligned to the tributary Ch.1 of two 160-Gbit/s signals. When the two pumps and S1 are present while S2 absent, Ch.1 of S1 is depleted

and converted to the Ch.1 of S2 with the proper adjustment of pump powers and polarization states due to the signal depletion and wavelength conversion effects. Similarly, as the two pumps and S2 are turned on while S1 off, Ch.1 of S2 is extinguished with its data information copied onto the Ch.1 of S1. In the presence of two 10-GHz pumps and both two 160-Gbit/s signals, Ch.1 of S2 is exchanged to the Ch.1 of S1. Meanwhile, Ch.1 of S1 is swapped to the Ch.1 of S2, resulting in the implementation of 10-Gbit/s tributary channel exchange between two 160-Gbit/s signals. Moreover, it is convenient to further perform the 10-Gbit/s tributary exchange for all 16 tributary channels of two 160-Gbit/s signals simply by time shifting the 10-GHz clock pumps to be aligned with the corresponding tributary channel of interest.
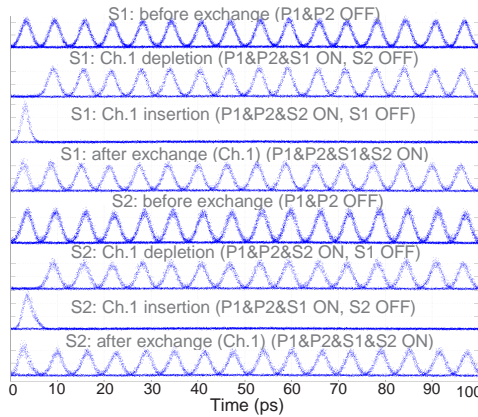

Figure 7. Measured eye diagrams for the tributary channel exchange (Ch. 1).

Figure 8 depicts power penalties at a BER of 10^{-9} of tributary exchange between two 160-Gbit/s signals for all 16 tributary channels. During the tributary channel exchange between two 160-Gbit/s signals, the average power penalty and the fluctuation of 16 tributary channels is around 3.7 and 1.1 dB for S1 (S2 to S1) and 3.9 and 1.1 dB for S2 (S1 to S2).
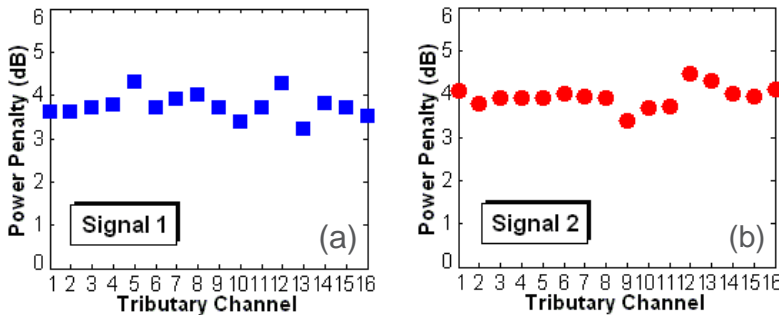

Figure 8. Power penalties of tributary exchange for 16 tributary channels. (a)(c) Signal 1. (b)(d) Signal 2.

3.2. Modulation-format-transparent data exchange using non-degenerate FWM in an HNLF [38-41]

In addition to cSFG/DFG ($\chi^{(2)} : \chi^{(2)}$) in a PPLN waveguide [22-26], signal depletion and wavelength conversion of non-degenerate FWM ($\chi^{(3)}$) in an HNLF can also enable the data exchange [29-41]. As shown in Fig. 9(a), when signal 1 (S1: λ_{S1}) and two continuous-wave (CW) pumps (P1: λ_{P1}, P2: λ_{P2}) are sent through the HNLF with S1 and P1 set symmetrically with respect to the zero-dispersion wavelength (ZDW) of the HNLF, S1 and P1 photons are consumed to produce photons of signal 2 (S2: λ_{S2}) and P2 during the non-degenerate FWM process. Thus the depletion of S1 is expected with its data information transparently copied onto a newly generated S2. Similarly, as shown in Fig. 9(b), the depletion of S2 accompanied by the generation of S1 can be achieved as S2 and two pumps are launched into the HNLF. As shown in Fig. 9(c), in the presence of two signals and two pumps at the input of HNLF with S1(S2) and P1(P2) symmetric relative to the ZDW of the HNLF, S1(S2) can be extinguished and converted to S2(S1), resulting in the implementation of data exchange between S1 and S2.
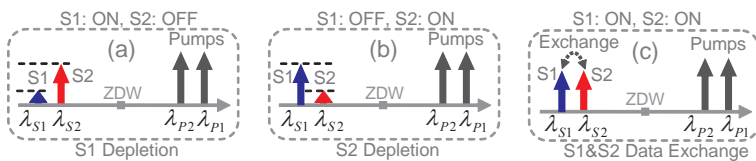

Figure 9. Concept and principle of non-degenerate FWM-based signal depletion and data exchange. (a) S1 depletion. (b) S2 depletion. (c) S1 & S2 data exchange.

For non-degenerate FWM-based data exchange, pump phase modulation is adopted in the experiment to suppress the stimulated Brillouin scattering (SBS) effect so that pump power can be efficiently utilized. Previous works of non-degenerate FWM-based data exchange have been reported for OOK signals [29-37], which are not affected by the phase modulation of two pumps. Shown in Fig. 10 is an example of data exchange (i.e., wavelength exchange) for 10-Gbit/s non-return-to-zero (NRZ) signals [32]. In order to perform phase-transparent data exchange for DPSK/DQPSK signals, it is desired that non-degenerate FWM-based data exchange has the characteristic of modulation-format-transparency.
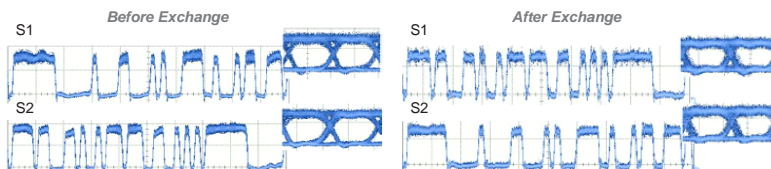

Figure 10. Results of data exchange (wavelength exchange) for 10-Gbit/s NRZ signals [32].

Under the non-depletion approximation, we derive the analytical solutions for the non-degenerate FWM involving two signals and two pumps written as [39]

$$A_{SA}^{'} = \left\{ A_{SA0}\left[\cos(gz) - \frac{ik\sin(gz)}{2g}\right] + A_{SB0}\frac{2i\gamma}{g}A_{P10}^{*}A_{P20}\sin(gz) \right\} e^{i\left[2\gamma(P_{10}+P_{20})+\frac{k}{2}\right]z} \quad \text{(a)}$$

$$A_{SB}^{'} = \left\{ A_{SA0}\frac{2i\gamma}{g}A_{P10}A_{P20}^{*}\sin(gz) + A_{SB0}\left[\cos(gz) + \frac{ik\sin(gz)}{2g}\right] \right\} e^{i\left[2\gamma(P_{10}+P_{20})-\frac{k}{2}\right]z} \quad \text{(b)}$$

(5)

where $g = \sqrt{4\gamma^2 P_{10}P_{20} + k^2/4}$ and $k = \Delta\beta + \gamma(P_{10}-P_{20})$ are constants related to the pump powers (P_{10}, P_{20}), nonlinear coefficient (γ), and phase mismatching ($\Delta\beta$). A_{SA0}, A_{SB0}, A_{P10} and A_{P20} are the complex amplitudes of input signals (SA, SB) and pumps (P1, P2) containing both amplitude and phase information. $A_{SA}^{'}$ and $A_{SB}^{'}$ are the complex amplitudes of output signals (SA, SB) after the data exchange. Under the exchange condition of phase matching ($k = 0$) and $gz = (N + 1/2)\pi$ ($N = 0, 1, 2, ...$) enabled by the proper adjustment of pump powers, we can further simplify Eqs. (5a)(5b) as follows

$$A_{SA}^{'} = \pm A_{SB0}\frac{2i\gamma}{g}A_{P10}^{*}A_{P20}e^{i2\gamma(P_{10}+P_{20})z} \quad \text{(a)}$$

$$A_{SB}^{'} = \pm A_{SA0}\frac{2i\gamma}{g}A_{P10}A_{P20}^{*}e^{i2\gamma(P_{10}+P_{20})z} \quad \text{(b)}$$

(6)

Note that Eqs. (6a)(6b) indicate the linear relationship of complex amplitude between the output and input signals ($A_{SA}^{'} \propto A_{SB0}$, $A_{SB}^{'} \propto A_{SA0}$), implying the implementation of phase-transparent optical data exchange. We can further obtain the corresponding phase relationships of $\phi_{SA}^{'} = \phi_{SB} + \phi_{P2} - \phi_{P1}$ and $\phi_{SB}^{'} = \phi_{SA} + \phi_{P1} - \phi_{P2}$. Remarkably, the pump phase transfer ($\phi_{P1} - \phi_{P2} \neq 0$) to the exchanged signals does not impact on the OOK data exchange but could cause severe degradation on the DPSK/DQPSK data exchange. Fortunately, according to the deduced phase relationships, it is possible to cancel the pump phase transfer by applying the precisely identical phase modulation to the two pumps (i.e., $\phi_{P1} = \phi_{P2}$), which makes it applicable to implement the data exchange of DPSK/DQPSK signals [38-41].

A 1-km piece of HNLF is adopted in the experiment, which has a nonlinear coefficient of 9.1 $W^{-1} \cdot km^{-1}$, a ZDW of ~1552 nm, and a fiber loss of 0.45 dB/km. To suppress SBS, identical phase modulation is applied to the two pumps using a single phase modulator (PM) driven by a 10-Gbit/s pseudo-random binary sequence (PRBS). According to Eqs. (6a)(6b), the precisely identical phase modulation of the two pumps could be canceled in the output signals after data exchange.

We demonstrate the phase-transparent data exchange between two 100-Gbit/s 2^7-1 PRBS return-to-zero DQPSK (RZ-DQPSK) signals (S1: signal 1, S2: signal 2) [40, 41]. Figure 11(a) displays the measured temporal waveforms of the demodulated in-phase (Ch. I) and quadrature (Ch. Q) components for the 100-Gbit/s RZ-DQPSK data exchange. It can be clear-

ly observed that the data information carried by two 100-Gbit/s RZ-DQPSK signals is suc-
cessfully swapped after the non-degenerate FWM-based data exchange. Figure 11(b) and (c)
plot BER curves for the 100-Gbit/s RZ-DQPSK data exchange. Less than 1.2-dB power penal-
ty at a BER of 10^{-9} is obtained for the 100-Gbit/s RZ-DQPSK wavelength conversion (WC)
with only one signal (S1 or S2) present. Less than 5-dB power penalty at a BER of 10^{-9} is ob-
served for the 100-Gbit/s RZ-DQPSK data exchange. The extra power penalty of data ex-
change compared to wavelength conversion could be ascribed to the beating effect between
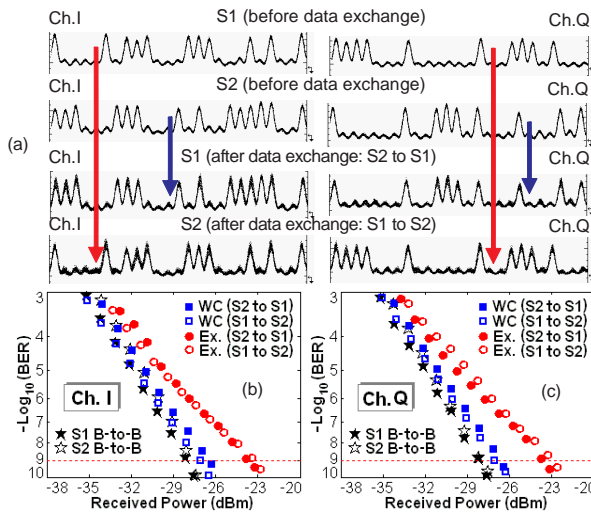the newly converted signal and the original residual signal.

Figure 11. Measured (a) demodulated waveforms and (b)(c) BER curves for 100-Gbit/s RZ-DQPSK data exchange.

3.3. Multi-channel data exchange using bidirectional degenerate FWM in an HNLF [42-45]

The aforementioned signal depletion and wavelength conversion based schemes with two
pumps enable the two-channel data exchange [22-26, 29-41]. However, the extended applica-
tions to simultaneous multi-channel data exchange might be limited. A laudable goal would
be to explore the data exchange between multi-channel signals.

Figure 12 illustrates the concept and principle of multi-channel data exchange [42, 43]. De-
generate FWM with a single CW pump is utilized. Four-channel DQPSK signals (S1-S4) are
symmetric with respect to the CW pump. Simultaneous data exchange between S1 and S4 as
well as S2 and S3 is expected. In general, such exchange function is not applicable with the
unidirectional degenerate FWM in a single HNLF since the newly converted signals cannot
be separated from the original signals. A potential solution is to explore the bidirectional de-
generate FWM in a single HNLF assisted by optical filtering. As shown in Fig. 12, for the
input four-channel signals (S1-S4), the filtered S1, S2 and CW pump are sent to HNLF from
the left side, yielding S4 and S3 via degenerate FWM. The newly generated S4 and S3 are

selected at the right side of HNLF while the original S1, S2 and CW pump are blocked. Meanwhile, the filtered S3, S4 and CW pump are fed into HNLF from the right side, producing S2 and S1 by degenerate FWM. The newly converted S2 and S1 are selected at the left side of HNLF while the original S3, S4 and CW pump are removed. As a consequence, simultaneous four-channel data exchange (S1&S4, S2&S3) can be achieved using bidirectional FWM in a single HNLF assisted by optical filtering. The combined S1-S4 from both sides of HNLF are the output four-channel signals after data exchange. Note that the in-phase (Ch. I) and quadrature (Ch. Q) components of DQPSK signals are swapped after data exchange due to the phase-conjugation characteristic of degenerate FWM.
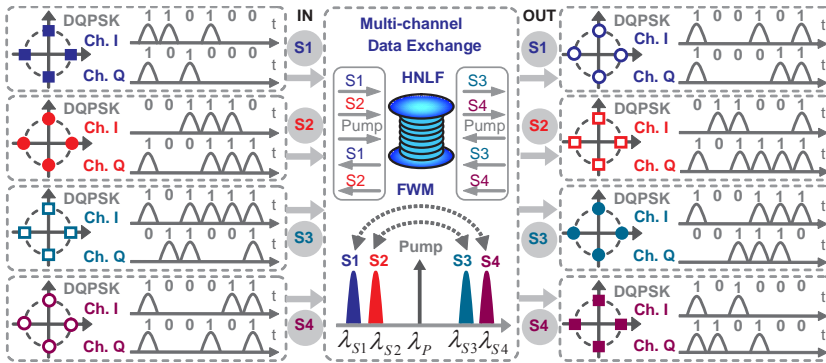

Figure 12. Concept and principle of simultaneous multi-channel DQPSK data exchange.

The proposed simultaneous multi-channel data exchange can be incorporated in a reconfigurable network switching element to enhance the efficiency and flexibility of optical networks. We construct a reconfigurable Tbit/s network switching element using double-pass liquid crystal on silicon (LCoS) technology accompanied by bidirectional degenerate FWM in a single HNLF. We demonstrate the LCoS+HNLF-based 2.3-Tbit/s multi-functional grooming switch which performs simultaneous selective add/drop, switchable data exchange, and power equalization, for 23-channel 100-Gbit/s RZ-DQPSK signals [44, 45].

ITU-grid-compatible 23-channel (from S1: 1531.12 nm to S23: 1566.31 nm) 100-Gbit/s RZ-DQPSK signals are employed in the experiment. Figure 13 shows the measured spectrum of the input unequalized 23-channel 100-Gbit/s RZ-DQPSK signals with a power fluctuation of ~9.1 dB. Shown in the insets are typical balanced eyes for the in-phase (Ch. I) and quadrature (Ch. Q) components.

Shown in Fig. 14 is the measured spectrum and balanced eyes after grooming switch with power equalization (<1 dB) for all 23 channels (input unequalization: ~9.1 dB), two-channel add/drop for S6 and S7, and simultaneous six-channel data exchange (S10, S11, S12, S21, S22, S23). The inset of Fig. 14 depicts the spectrum of dropped S6 and S7. The BER performance is plotted in Fig. 15 and power penalties less than 5 dB for six-channel data exchange are observed at a BER of 10⁻⁹.
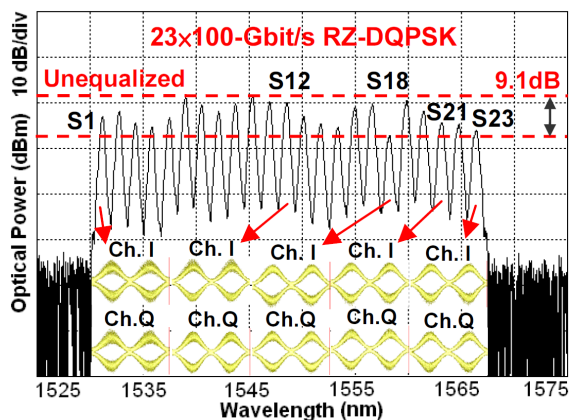
Figure 13. Measured spectrum and balanced eyes for input unequalized 23-channel 100-Gbit/s RZ-DQPSK signals.
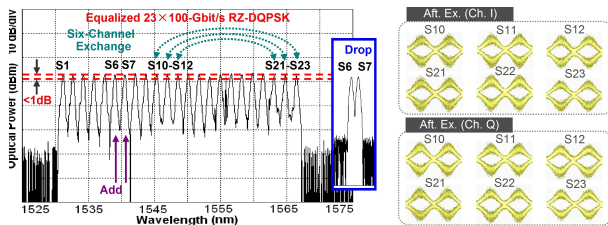

Figure 14. Measured spectrum and balanced eyes after multi-functional grooming switch (S6, S7: add/drop; S10, S11, S12, S21, S22, S23: data exchange; S1-S23: power equalization).
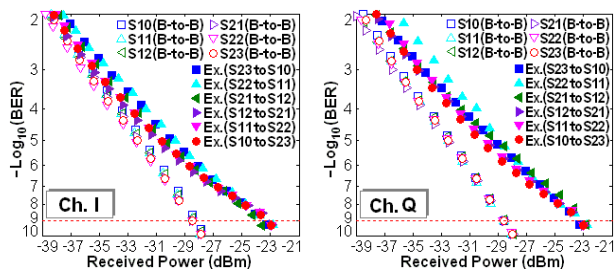

Figure 15. BER curves for simultaneous six-channel data exchange (S10, S11, S12, S21, S22, S23).

3.4. Data exchange between two orthogonal polarizations using kerr-induced nonlinear polarization rotation in an HNLF [48, 49]

In addition to the data exchange in the wavelength and time domains [22-45], it is also possible to perform data exchange between two orthogonal polarizations in the time and polari-

zation domains [48-50]. We experimentally demonstrate the orthogonal tributary channel exchange between two pol-muxed DPSK OTDM data streams by using the Kerr effect-induced nonlinear birefringence in an HNLF [48, 49].

Figure 16 illustrates the concept and principle of the Kerr effect-based orthogonal tributary channel exchange of a pol-muxed DPSK OTDM signal. The strong subrate clock pump is 45° linearly polarized with respect to the two orthogonal polarizations of a pol-muxed DPSK OTDM signal. With the help of proper pump power control, the pump-induced nonlinear birefringence by Kerr effect could bring the selected tributary channel (aligned with the subrate clock pump) to a 90° polarization rotation for both of the two orthogonal polarizations of the pol-muxed signal, leading to the orthogonal tributary channel exchange when the pump is present. Other unselected orthogonal tributary channels with the pump absent will not experience the nonlinear polarization rotation and hence will be untouched. In addition, simply by shifting the subrate clock pump to be aligned with the tributary channel of interest, it is possible to implement orthogonal tributary channel exchange for all tributary channels of the pol-muxed DPSK OTDM signal.
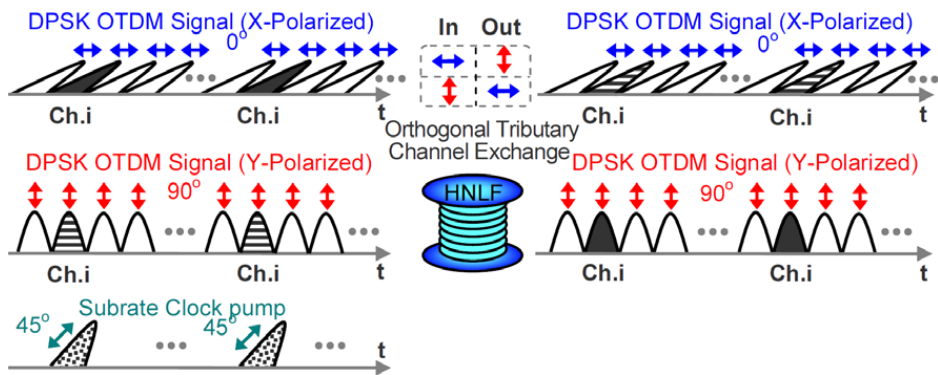

Figure 16. Concept and principle of Kerr effect-based orthogonal tributary channel exchange of a pol-muxed DPSK OTDM signal.

Figure 17 displays the eye diagrams measured by an optical sampling scope for the typical orthogonal tributary channel (Ch. 1) exchange of a 160-Gbit/s pol-muxed DPSK OTDM signal. As the 10-GHz clock pump is time aligned to tributary channel 1 (Ch. 1) of the X- and Y-polarized DPSK OTDM signal, in the absence of the Y-polarization, as shown in Fig. 17(b), Ch. 1 of the X-polarization is blocked by an X-polarizer after the HNLF due to the 90° rotation from the X- to the Y-polarization. When the Y-polarization is present but the X-polarization is absent, Ch. 1 of the Y-polarization is inserted to the X-polarization through the 90° rotation from the Y- to the X-polarization, as shown in Fig. 17(c). In the presence of both the X- and Y-polarizations, the tributary Ch. 1 of the Y-polarization is changed to the X-polarization, as shown in Fig. 17(d). Meanwhile, the original tributary Ch. 1 of the X-polarization is

also changed to the Y-polarization, as shown in Fig. 17(h), resulting in the orthogonal tributary channel exchange of a pol-muxed DPSK OTDM signal.
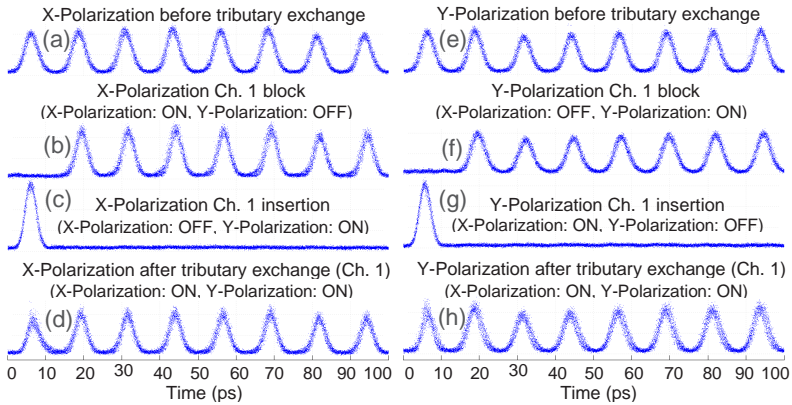

Figure 17. Eye diagrams of orthogonal tributary channel (Ch. 1) exchange of a 160-Gbit/s pol-muxed DPSK OTDM signal.

Figure 18 plots the power penalties of the orthogonal tributary exchange for 8 tributary channels. Less than 4-dB power penalty at a BER of 10^{-9} is obtained for all 8 tributary channels with a fluctuation of <1.5 dB.
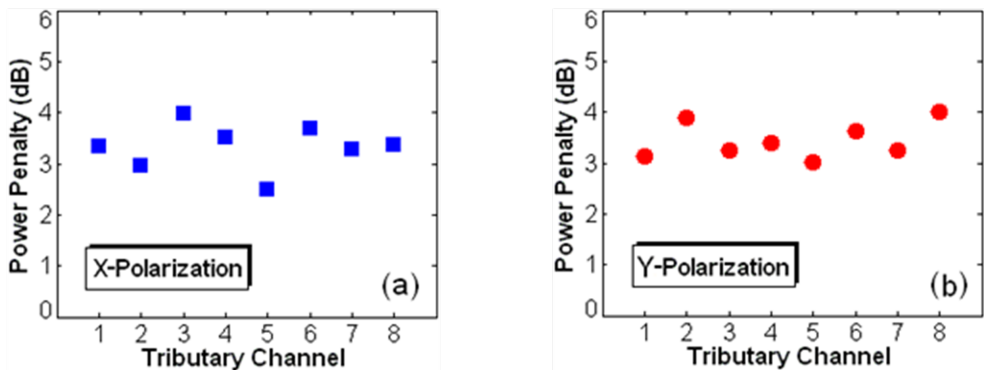

Figure 18. Power penalties of orthogonal tributary exchange for 8 tributary channels.

3.5. Time-slot-exchange using conversion-dispersion-based tunable delays [46, 47]

The demonstrated data exchange of groups of bits or tributary channels manipulates data in multiple degrees of freedom, such as time- (groups of bit) and channel-selective data exchange between WDM channels [23, 24], tributary channel exchange between two WDM

high-speed OTDM signals [25, 26], and orthogonal tributary channel exchange of a pol-muxed OTDM signal [48-50]. Another important traffic grooming function, known as time-slot exchange or time-slot interchange, is to manipulate data only in the time domain to enable contention resolution and increase throughput efficiency in time-based networks. Time-slot exchange, occurring on the bit or packet level, can afford the network enhanced flexibility. For packet-switched networks, exchanging full data packets in the time domain requires optical delays that are tunable.

Figure 19 shows concept and principle of conversion-dispersion-based time-slot exchange of two separate packets in the time domain [46]. Three clocked pumps (λ_{P1}, λ_{P2}, λ_{P3}) are fed into an HNLF, along with a packetized input signal (λ_S) located near the ZDW of HNLF. Degenerate FWM between the clocked pumps and signal generates replicas of the input signal at new converted wavelengths (λ_1, λ_2, λ_3) which contain only the information of the input signal at times when the clocked pumps are on. The three pumps are clocked to convert: (i) only packet A to λ_1, (ii) all information but packets A and B to λ_2, and (iii) only packet B to λ_3. The three converted signals (λ_1, λ_2, λ_3) then pass through a dispersion module, such as dispersion compensation fiber (DCF), and experience a wavelength-dependent delay via inter-channel chromatic dispersion. Due to the conversion-dispersion-based tunable delays, packet A is advanced, while packet B is retarded, relative to the reference (all information but packets A and B), resulting in the swapping of packets A and B in the time domain. After the delays, all three converted signals are converted back to the original signal wavelength using a PPLN waveguide followed by the compensation for intra-channel chromatic dispersion.
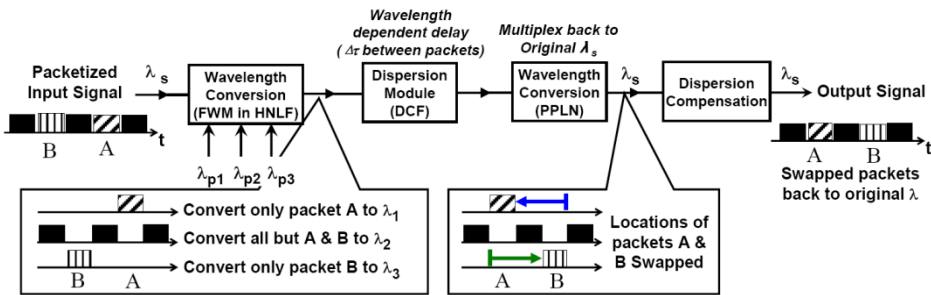

Figure 19. Concept and principle of time-slot exchange of two separate packets using conversion-dispersion-based tunable delays.

Shown in Figs. 20 and 21 are experimental results of time-slot exchange of 40-Gbit/s optical data packets using conversion-dispersion-based tunable delays. Separate 182-bit packets are converted to separate wavelengths, delayed relative to one another using conversion-dispersion-based tunable delays, and then recombined together to achieve new packets with time slots exchanged.

Similarly, time-slot exchange between odd and even data packets is also achievable using conversion-dispersion-based tunable delays [47]. As illustrated in Fig. 22, odd and even data

packets are extracted from an input signal via wavelength multicasting with clocked pumps, delayed relative to one another in a dispersion module, and then multiplexed back together using wavelength conversion in a PPLN waveguide followed by dispersion compensation. Shown in Fig. 23 are experimental results of time-slot exchange of 40-Gbit/s odd and even packets. The conversion-dispersion-based tunable delays enable time-slot exchange of variable length optical packets (182 and 288 bits/packet).
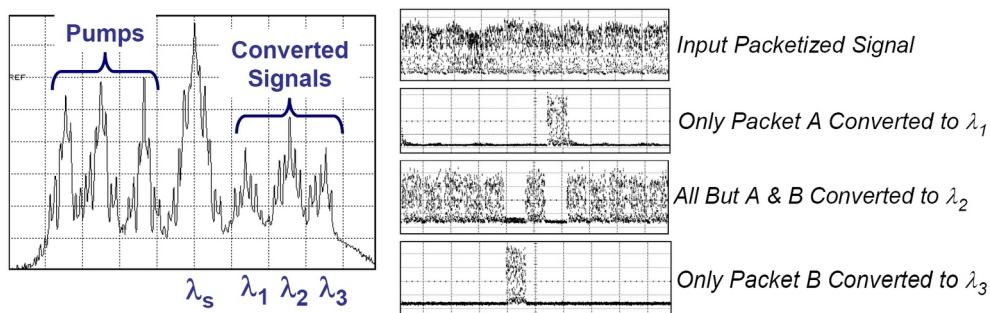

Figure 20. Optical spectra (left) and temporal waveforms (right) of converted signals after multicasting using clocked pumps in HNLF.
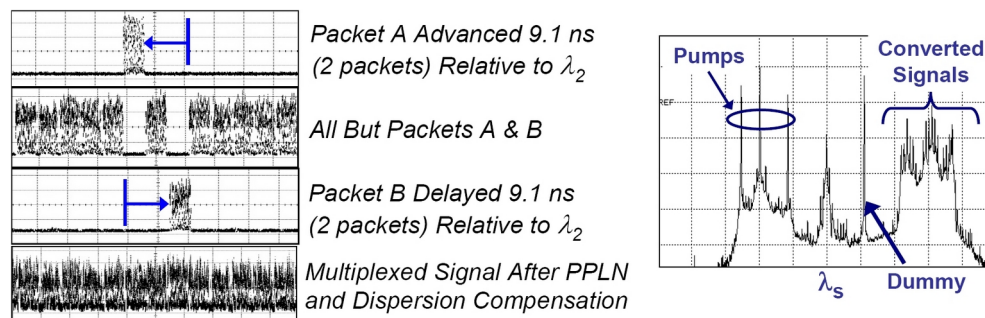

Figure 21. Temporal waveforms of optical signals following delay via dispersion, conversion back to the original signal wavelength and dispersion compensation (left) and optical spectra after PPLN (right).

3.6. Data exchange between "twisted" light beams carrying Orbital Angular Momentum (OAM) [51, 52]

In optical communications, beyond well-known existing degrees of freedom such as wavelength, time and polarization, other degrees of freedom are encouraged to be explored to break "capacity crunch". For example, OAM which is related to the helical phase front of "twisted" light beams [59-61], can be considered as an additional degree of freedom [62, 63], where the multiplexing of data-carrying OAM beams provides yet another dimension in the

ever-continuing effort to increase the capacity and spectral efficiency of communication links [63]. When employing OAM beams to carry data information, a desirable function for flexible data processing would be the data exchange between "twisted" OAM beams.
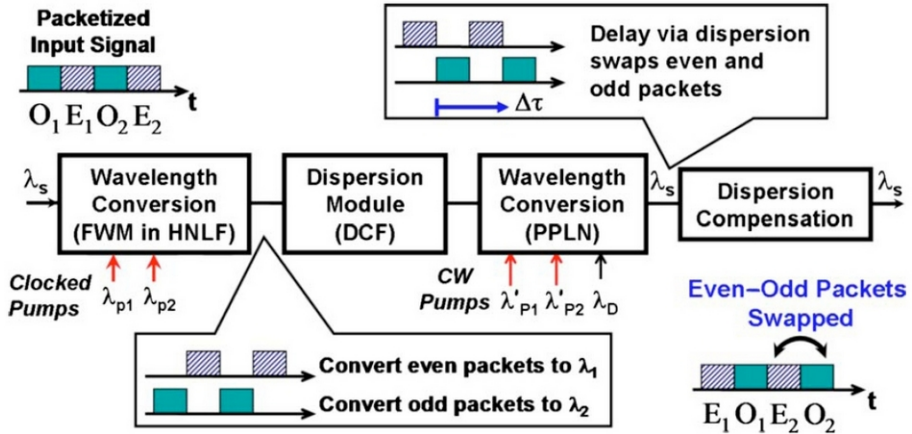

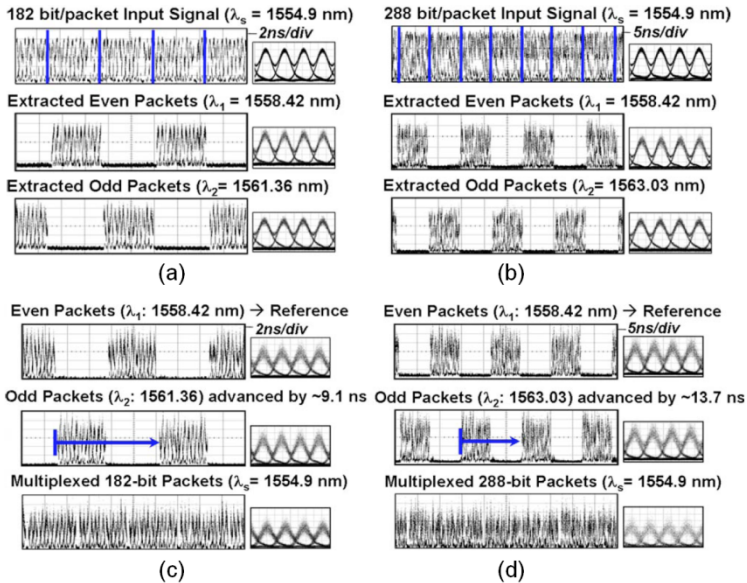**Figure 22.** Concept and principle of time-slot exchange of odd and even packets.

Figure 23. Temporal waveforms of time-slot exchange of 40-Gbit/s odd and even packets with two variable packet lengths. (a)(c) 182 bits/packet. (b)(d) 288 bits/packet.
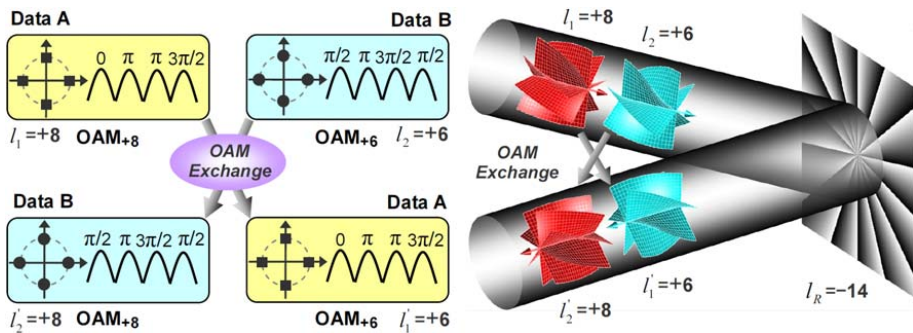
Figure 24. Concept and principle of data exchange between "twisted" OAM beams.

Figure 24 shows concept and principle of data exchange between OAM beams [51, 52]. Superposed two OAM beams (OAM_{ℓ_1}, OAM_{ℓ_2}), each carrying different data information (Signal A, Signal B), shine at a reflective-type spatial light modulator (SLM) loaded with a spiral phase mask with a charge of $\ell_R = -(\ell_1 + \ell_2)$. After reflecting off the SLM, this phase mask adds an azimuthal phase term $\exp(i\ell_R\theta)$ to the two OAM beams and converts them into $OAM_{-\ell_2}$ and $OAM_{-\ell_1}$, which are further transformed into OAM_{ℓ_2} and OAM_{ℓ_1} due to reflection of the SLM which flips the charge sign. As a result, data exchange between two OAM beams is implemented. For the input of two OAM beams with varied charges, reconfigurable data exchange is available by updating the phase mask loaded into the reflective-type SLM. Shown in Fig. 24 is an example of data exchange between DQPSK-carrying "twisted" OAM beams (OAM_{+8}, OAM_{+6}).

The measured interferograms (i.e., interference between OAM beams and a reference Gaussian beam), as shown in Fig. 25(a) and (b), indicate that the charges of two OAM beams before exchange are +8 and +6. After exchange, the measured interferograms, as shown in Fig. 25(c) and (d), verify that the charges of two OAM beams after exchange become +6 and +8 (see Ref. 52 for details). Figure 25(e)-(h) show measured interferograms of reconfigurable data exchange between another two OAM beams (OAM_{+10} and OAM_{+6}) by updating the spiral phase mask loaded into the SLM.

We measure temporal waveforms and balanced eyes of demodulated in-phase (Ch. I) and quadrature (Ch. Q) components of 100-Gbit/s RZ-DQPSK signals. As shown in Fig. 26, the observed temporal waveforms confirm the successful implementation of data exchange between two OAM beams (OAM_{+10} and OAM_{+6}). Shown in Fig. 27 are measured BER curves for 100-Gbit/s RZ-DQPSK data exchange between OAM_{+10} and OAM_{+6} beams with power penalty <1.9-dB at a BER of $1e^{-9}$.
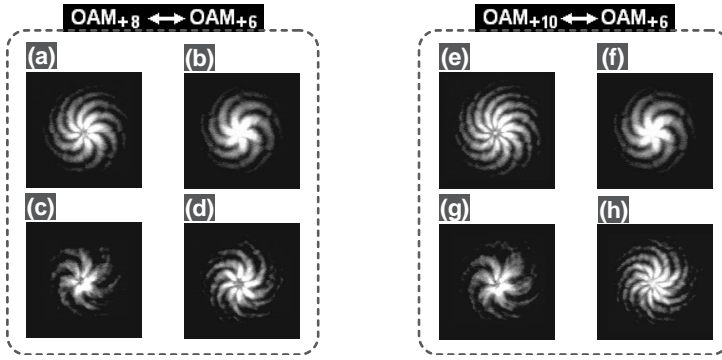
Figure 25. Measured interferograms. (a) OAM_{+8} and (b) OAM_{+6} beams become (c) OAM_{+6} and (d) OAM_{+8} ones after exchange. (e) OAM_{+10} and (f) OAM_{+6} beams become (g) OAM_{+6} and (h) OAM_{+10} ones after exchange.
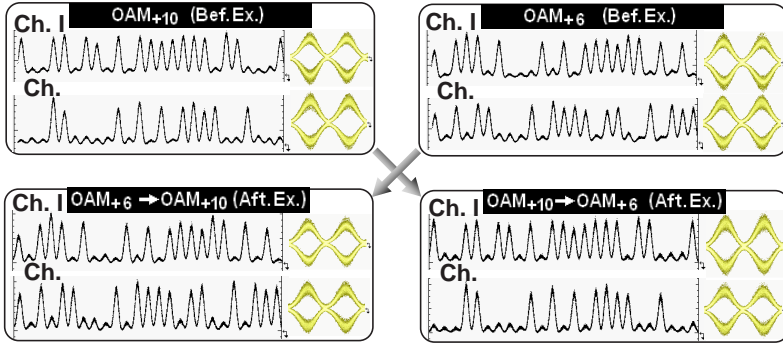

Figure 26. Measured waveforms and balanced eyes of demodulated in-phase (Ch. I) and quadrature (Ch. Q) components of 100-Gbit/s RZ-DQPSK signals for data exchange between OAM_{+10} and OAM_{+6} beams. Bef. Ex., before exchange; Aft. Ex., after exchange.
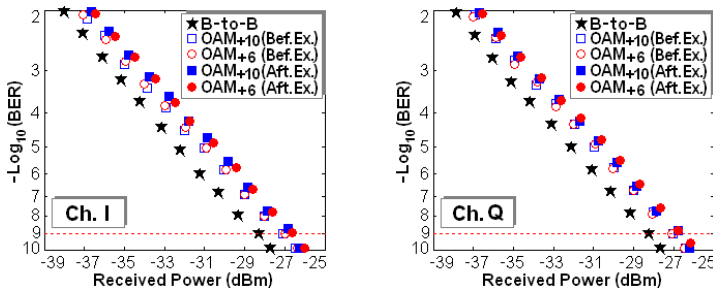

Figure 27. Measured BER curves for 100-Gbit/s RZ-DQPSK data exchange between OAM_{+10} and OAM_{+6} beams.

4. Discussions

The demonstrated miscellaneous data exchange functionalities provide great potential for facilitating flexible networks. With future improvement, several aspects could be considered as follows.

1. In practical applications, some supplementary functionalities might be required to construct complete and independent data exchange modules. Taking tributary channel exchange as an example (Figs. 6-8), subrate clock pumps should be synchronized with high-speed OTDM signals. Note that the incoming signals and locally generated pumps are usually independent with each other. Hence, a supplementary functionality of clock recovery is required in real situations to get synchronized subrate clock pumps from incoming signals. Fortunately, various optical clock recovery methods have been developed [64]. In particular, recent promising demonstrations have shown the successful synchronization and sub-clock recovery for ultra-high speed OTDM signals up to 640 Gbit/s [65, 66]. As a consequence, it is possible develop a complete and independent data exchange module by incorporating a synchronization and clock recovery unit.

2. Beyond reported functionalities, data exchange can be further extended in terms of degrees of freedom, modulation formats, and granularities. For example, some additional degrees of freedom have recently attracted increasing interest in high-speed optical fiber communications to break the "capacity crunch", such as space [67, 68] and mode [69, 70]. A valuable goal would be achieve data exchange in these degrees of freedom. Also, some high-level modulation formats have been used in fiber transmission, such as 16-ary quadrature amplitude modulation (16-QAM), 32-QAM, etc [67, 68, 71]. According to the demonstrated characteristic of modulation-format-transparency, most of the presented data exchange should be, in principle, available for these advanced modulation formats. However, high-level modulation formats show reduced tolerable performance degradation, and therefore accurate manipulation of amplitude and phase would be expected. Additionally, data exchange with fine granularity in the time domain requires accurate control of time delay, which could be achievable assisted by the fine tuning of conversion-dispersion-based optical delays [7].

3. In addition to PPLN and HNLFs, there would be some other alternative candidates applicable for data exchange, including the use of third-order nonlinearities in semiconductor optical amplifiers (SOAs) [3], As_2S_3 waveguides [19], and silicon waveguides [18].

5. Conclusion

In this chapter, we have reviewed recent research efforts towards robust data exchange. Various kinds of optical nonlinearities, i.e., cSFG/DFG in a PPLN waveguide, non-degenerate FWM in an HNLF, bidirectional degenerate FWM in an HNLF, Kerr-induced nonlinear po-

larization rotation in an HNLF, and conversion-dispersion-based tunable delays, together with simple linear optics, are exploited to enable robust data exchange in different degrees of freedom (wavelength, time, polarization, phase front), for different modulation formats (OOK, DPSK, DQPSK, pol-muxed), and at different granularities (entire data, groups of bits, tributary channels).

First, analytical solutions to the single-PPLN-based data exchange are derived showing the exchange condition. 40-Gbit/s time- (groups of bits) and channel-selective data exchange between four WDM channels is implemented. 10-Gbit/s tributary channel exchange between two WDM 160-Gbit/s OTDM signals is demonstrated. Second, analytical solutions to the non-degenerate FWM-based data exchange are derived indicating the exchange condition and implying the characteristic of modulation-format-transparency. Phase-transparent data exchange (entire data) of 100-Gbit/s RZ-DQPSK signals is demonstrated. Third, a simple approach is proposed to perform simultaneous multi-channel data exchange using bidirectional degenerate FWM in an HNLF. A reconfigurable Tbit/s network switching element is constructed using double-pass LCoS technology, together with bidirectional degenerate FWM in a single HNLF. LCoS+HNLF-based 2.3-Tbit/s (23X100-Gbit/s RZ-DQPSK) multi-functional grooming switch (e.g., simultaneous add/drop, six-channel data exchange, and power equalization) is implemented. Fourth, 10-Gbit/s tributary channel exchange between two orthogonal polarizations of a 160-Gbit/s pol-muxed DPSK OTDM signal is demonstrated based on the Kerr-induced nonlinear polarization rotation. Fifth, time-slot exchange of 40-Gbit/s optical data packets is demonstrated using conversion-dispersion-based tunable delays. Finally, reconfigurable 100-Gbit/s RZ-DQPSK data exchange between "twisted" OAM beams is demonstrated using simple linear optics.

The obtained theoretical and experimental results of data exchange in the wavelength, time, polarization and phase front domains, show that robust data exchange for different modulation formats and at different granularities could potentially enhance the efficiency and flexibility of optical networks.

Acknowledgements

Author details

Jian Wang[1*] and Alan E. Willner[2]

*Address all correspondence to: jwang@hust.edu.cn

1 Wuhan National Laboratory for Optoelectronics, College of Optoelectronic Science and Engineering, Huazhong University of Science and Technology, Wuhan, Hubei, China

2 Department of Electrical Engineering, University of Southern California, Los Angeles, California, USA

References

[1] Saruwatari M. All-optical signal processing for terabit/second optical transmission. IEEE J. Sel. Top. Quantum Electron. 2000; 6(6): 1363-1374.

[2] Yoo SJB Wavelength conversion technologies for WDM network applications. J. Lightwave Technol. 1996; 14(6): 955-966.

[3] Chan K, Chan CK, Chen LK, Tong F. Demonstration of 20-Gb/s all-optical XOR gate by four-wave mixing in semiconductor optical amplifier with RZ-DPSK modulated inputs. IEEE Photon. Technol. Lett. 2004; 16(3): 897-899.

[4] Wang J, Sun JQ, Zhang XL, Huang DX, Fejer MM. All-optical format conversions using periodically poled lithium niobate waveguides. IEEE J. Quantum Electron. 2009; 45(2): 195-205.

[5] Okawachi Y, Sharping JE, Xu C, Gaeta AL. Large tunable optical delays via self-phase modulation and dispersion. Opt. Express 2006; 14(25): 12022-12027.

[6] Wang Y, Yu CY, Yan LS, Willner AE, Roussev R, Langrock C, Fejer MM, Sharping JE, Gaeta AL. 44-ns continuously tunable dispersionless optical delay element using a PPLN waveguide with two-pump configuration, DCF, and a dispersion compensator. IEEE Photon. Technol. Lett. 2007; 19(11): 861-863.

[7] Nuccio SR, Yilmaz OF, Wu X, Willner AE. Fine tuning of conversion/dispersion based optical delays with a 1 pm tunable laser using cascaded acousto-optic mixing. Opt. Lett. 2010; 35(4): 523-525.

[8] Dai Y, Okawachi Y, Turner-Foster AC, Lipson M, Gaeta AL, Xu C. Ultralong continuously tunable parametric delays via a cascading discrete stage. Opt. Express 2010; 18(1): 333-339.

[9] Salem R, Foster MA, Turner AC, Geraghty DF, Lipson M, Gaeta AL. Signal regeneration using low-power four-wave mixing on silicon chip. Nature Photonics 2008; 2(1): 35-38.

[10] Kataoka N, Sone K, Wada N, Aoki Y, Kinoshita S, Miyata H, Miyazaki T, Onaka H, Kitayama K. Field trial of 640-Gbit/s-throughput, granularity-flexible optical network using packet-selective ROADM prototype. J. Lightwave Technol. 2009; 27(7): 825-832.

[11] Wang J, Fu HY, Geng DY, Willner AE. All-optical wavelength-/time-selective switching/dropping/swapping for 100-GHz-spaced WDM signals using a periodically poled lithium niobate waveguide. ECOC2012, paper Th.1.A.5, 2012.

[12] Wu XX, Bogoni A, Yilmaz OF, Nuccio SR, Wang J, Willner AE. Eightfold 40-320 Gbit/s phase-coherent multiplexing and 320-40 Gbit/s demultiplexing using highly nonlinear fibers. Opt. Lett. 2010; 35(11): 1896-1898.

[13] Brès CS, Boggio JMC, Alic N, Radic S. 1-to-40 10-Gb/s channel multicasting and amplification in wideband parametric amplifier. IEEE Photon. Technol. Lett. 2008; 20(16): 1417-1419.

[14] Biberman A, Lee BG, Turner-Foster AC, Foster MA, Lipson M, Gaeta AL, Bergman K. Wavelength multicasting in silicon photonic nanowires. Opt. Express 2010; 18(17): 18047-18055.

[15] Hamza HS, Deogun JS. Wavelength-exchanging cross connects (WEX)—a new class of photonic cross-connect architectures. J. Lightwave Technol. 2006; 24(3): 1101-1111.

[16] Winzer PJ, Essiambre RJ. Advanced optical modulation formats. Proc. IEEE 2006; 94(5): 952-985.

[17] Winzer PJ, Essiambre RJ. Advanced modulation formats for high-capacity optical transport networks. J. Lightwave Technol. 2006; 24(23): 4711-4728.

[18] Oxenløwe LK, Ji H, Galili M, Pu MH, Hu H, Mulvad, HCH, Yvind K, Hvam JM, Clausen AT, Jeppesen P. Silicon photonics for signal processing of Tbit/s serial data signals. IEEE J. Sel. Top. Quantum Electron. 2012; 18(2): 996-1005.

[19] Pelusi MD, Ta'eed VG, Fu LB, Mägi E, Lamont MRE, Madden S, Choi DY, Bulla DAP, Luther-Davies B, Eggleton BJ. Applications of highly-nonlinear chalcogenide glass devices tailored for high-speed all-optical signal processing. IEEE J. Sel. Top. Quantum Electron. 2008; 14(3): 529-539.

[20] Chowdhury A, Hagness SC, McCaughan L. Simultaneous optical wavelength interchange with a two-dimensional second-order nonlinear photonic crystal. Opt. Lett. 2000; 25(11): 832-834.

[21] Chowdhury A, Staus C, Boland BF, Kuech TF, McCaughan L. Experimental demonstration of 1535–1555 nm simultaneous optical wavelength interchange with a nonlinear photonic crystal. Opt. Lett. 2001; 26(17): 1353-1355.

[22] Wang J, Sun QZ. Theoretical analysis of power swapping in quadratic nonlinear medium. Appl. Phys. Lett. 2010; 96(8): 081108.

[23] Wang J, Nuccio SR, Wu XX, Yilmaz OF, Zhang L, Fazal I, Yang JY, Yue Y, Willner AE. 40-Gbit/s optical data exchange between WDM channels using second-order nonlinearities in PPLN waveguides. NLO 2009, paper PDPA1, 2009.

[24] Wang J, Nuccio SR, Wu XX, Yilmaz OF, Zhang L, Fazal I, Yang JY, Yue Y, Willner AE. 40 Gbit/s optical data exchange between wavelength-division-multiplexed channels using a periodically poled lithium niobate waveguide. Opt. Lett. 2010; 35(7): 1067-1069.

[25] Wang J, Bakhtiari Z, Xiao-Li Y, Yilmaz OF, Nuccio SR, Wu XX, Huang H, Yang JY, Yue Y, Fazal I, Hellwarth R, Willner AE. Experimental demonstration of data traffic grooming of a single 10-Gbit/s TDM tributary channel between two 160-Gbit/s WDM channels. OFC 2010, paper OWF1, 2010.

[26] Wang J, Bakhtiari Z, Yilmaz OF, Nuccio SR, Wu XX, Willner AE. 10 Gbit/s tributary channel exchange of 160 Gbit/s signals using periodically poled lithium niobate. Opt. Lett. 2011; 36(5): 630-632.

[27] Mori K, Takara H, Saruwatari M. Wavelength interchange with an optical parametric loop mirror. Electron. Lett. 1997; 33(6): 520-522.

[28] Gao Y, Dai YH, Shu C, He SL. Wavelength interchange of phase-shift-keying signal. IEEE Photon. Technol. Lett. 2010; 22(11): 838-840.

[29] Wong KKY, Marhic ME, Uesaka K, Kazovsky LG. Demonstration of wavelength exchange in a highly nonlinear fiber. ECOC 2001, pp. 272-273, 2001.

[30] Uesaka K, Wong KKY, Marhic ME, Kazovsky LG. Polarization-insensitive wavelength exchange in highly-nonlinear dispersion-shifted fiber. OFC2002, paper ThY3, 2002.

[31] Uesaka K, Wong KKY, Marhic ME, Kazovsky LG. Wavelength exchange in a highly nonlinear dispersion-shifted fiber: theory and experiments. IEEE J. Sel. Topics Quantum Electron. 2002; 8(3): 560-568.

[32] Fung RWL, Cheung HKY, Wong KKY. Widely tunable wavelength exchange in anomalous-dispersion regime. IEEE Photon. Technol. Lett. 2007; 19(22): 1846-1848.

[33] Cheung HKY, Fung RWL, Kwok CH, Wong KKY. All-optical packet switching by pulsed-pump wavelength exchange in a highly nonlinear dispersion-shifted fiber. OFC2007, paper OTuB4, 2007.

[34] Shen M, Xu X, Yuk TI, Wong KKY. Byte-level parametric wavelength exchange for narrow pulsewidth return-to-zero signals. IEEE Photon. Technol. Lett. 2009; 21(21): 1591-1593.

[35] Kwok CH, Kuo BPP, Wong KKY. Pulsed pump wavelength exchange for high speed signal de-multiplexing. Opt. Express 2008; 16(15): 10894-10899.

[36] Shen M, Xu X, Yuk TI, Wong KKY. A 160-Gb/s OTDM demultiplexer based on parametric wavelength exchange. IEEE J. Quantum Electron. 2009; 45(11): 1309-1316.

[37]   Shen M, Cheung HKY, Fung RWL, Wong KKY. A comprehensive study on the dynamic range of wavelength exchange and its impact on exchanged signal performance. J. Lightwave Technol. 2009; 27(14): 2707-2716.

[38]   Wang J, Bakhtiari Z, Xiao-Li Y, Nuccio SR, Yilmaz OF, Wu XX, Yang JY, Yue Y, Fazal I, Hellwarth R, Willner AE. Phase-transparent optical data exchange of 40-Gbit/s DPSK signals using four-wave-mixing in a highly nonlinear fiber. OFC 2010, paper OMT6, 2010.

[39]   Wang J, Bakhtiari Z, Nuccio SR, Yilmaz OF, Wu X, Willner AE. Phase-transparent optical data exchange of 40 Gbit/s differential phase-shift keying signals. Opt. Lett. 2010; 35(17): 2979-2981.

[40]   Wang J, Nuccio SR, Huang H, Wang X, Yilmaz OF, Wu XX, Yang JY, Yue Y, Willner AE. Demonstration of 100-Gbit/s DQPSK data exchange between two different wavelength channels using parametric depletion in a highly nonlinear fiber. ECOC 2010, paper Mo.1.A.4, 2010.

[41]   Wang J, Nuccio SR, Huang H, Wang X, Yang JY, Willner AE. Optical data exchange of 100-Gbit/s DQPSK signals. Opt. Express 2010; 18(23): 23740-23745.

[42]   Wang J, Huang H, Wang X, Yang JY, Willner AE. Optical phase-transparent data grooming exchange of multi-channel 100-Gbit/s RZ-DQPSK signals. IEEE 23rd Photonics Society Annual Meeting 2010, paper WN2, 2010.

[43]   Wang J, Huang H, Wang X, Yang JY, Willner AE. Multi-channel 100-Gbit/s DQPSK data exchange using bidirectional degenerate four-wave mixing. Opt. Express 2011; 19(4): 3332-3338.

[44]   Wang J, Huang H, Wang X, Yang JY, Yilmaz OF, Wu XX, Nuccio SR, Willner AE. 2.3-Tbit/s (23X100-Gbit/s) RZ-DQPSK grooming switch (simultaneous add/drop, data exchange and equalization) using double-pass LCoS and bidirectional HNLF. OFC 2011, paper OTuE2, 2011.

[45]   Wang J, Huang H, Wang X, Yang JY, Willner AE. Reconfigurable 2.3-Tbit/s DQPSK simultaneous add/drop, data exchange and equalization using double-pass LCoS and bidirectional HNLF. Opt. Express 2011; 19(19): 18246-18252.

[46]   Christen L, Yilmaz OF, Nuccio SR, Wu XX, Fazal I, Willner AE. Tunable time-slot-interchange of 40-Gb/s optical packets using conversion/dispersion-based tunable 100-ns delays. OFC2008, paper OThA4, 2008.

[47]   Yilmaz OF, Christen L, Wu XX, Nuccio SR, Fazal I, Willner AE. Time-slot interchange of 40 Gbit/s variable length optical packets using conversion-dispersion-based tunable delays. Opt. Lett. 2008; 33(17): 1954-1956.

[48]   Wang J, Yilmaz OF, Nuccio SR, Wu XX, Bakhtiari Z, Xiao-Li Y, Yang JY, Huang H, Yue Y, Fazal I, Hellwarth R, Willner AE. Data traffic grooming/exchange of a single 10-Gbit/s TDM tributary channel between two pol-muxed 80-Gbit/s DPSK channels. CLEO 2010, paper CFJ5, 2010.

[49] Wang J, Yilmaz OF, Nuccio SR, Wu XX, Willner AE. Orthogonal tributary channel exchange of 160-Gbit/s pol-muxed DPSK signal. Opt. Express 2010; 18(16): 16995-17008.

[50] Suzuki J, Taira K, Fukuchi Y, Ozeki Y, Tanemura T, Kikuchi K. All-optical time-division add-drop multiplexer using optical fibre Kerr shutter. Electron. Lett. 2004; 40(7): 445-446.

[51] Wang J, Willner AE. Review of robust data exchange using optical nonlinearities. International Journal of Optics 2012; 2012: Article ID 575429 doi: 10.1155/2012/575429.

[52] Wang J, Yang JY, Fazal IM, Ahmed N, Yan Y, Willner AE, Dolinar S, Tur M. Experimental demonstration of 100-Gbit/s DQPSK data exchange between orbital-angular-momentum modes. OFC2012, paper OW1I.5, 2012.

[53] Wang J, Yang JY, Fazal IM, Ahmed N, Yan Y, Huang H, Ren YX, Yue Y, Dolinar S, Tur M, Willner AE. Terabit free-space data transmission employing orbital angular momentum multiplexing. Nature Photonics 2012; 6(7): 488-496.

[54] Willner AE, Yilmaz OF, Wang J, Wu XX, Bogoni A, Zhang L, Nuccio SR. Optically efficient nonlinear signal processing. IEEE J. Sel. Topics Quantum Electron. 2011; 17(2): 320-332.

[55] Tian Y, Xiao XS, Gao SM, Yang CX. All-optical switch based on two-pump four-wave mixing in fibers without a frequency shift. Appl. Opt. 2007; 46(23): 5588-5592.

[56] Parameswaran KR, Fujimura M, Chou MH, Fejer MM. Low-power all-optical gate based on sum frequency mixing in APE waveguides in PPLN. IEEE Photon. Technol. Lett. 2000; 12(6): 654-656.

[57] Wang J, Sun JQ, Sun QZ. Experimental observation of a 1.5 μm band wavelength conversion and logic NOT gate at 40 Gbit/s based on sum-frequency generation. Opt. Lett. 2006; 31(11): 1711-1713.

[58] Wang J, Sun JQ, Sun QZ. Single-PPLN-based simultaneous half-adder, half-subtracter, and OR logic gate: proposal and simulation. Opt. Express 2007; 15(4): 1690-1699.

[59] Allen L, Beijersbergen MW, Spreeuw RJC, Woerdman JP. Orbital angular momentum of light and the transformation of Laguerre–Gaussian laser modes. Phys. Rev. A 1992; 45(11): 8185-8189.

[60] Franke-Arnold S, Allen L, Padgett M. Advances in optical angular momentum. Laser Photon. Rev. 2008; 2(4): 299-313.

[61] Yao AM, Padgett MJ. Orbital angular momentum: origins, behavior and applications. Adv. Opt. Photon. 2011; 3(2): 161-204.

[62] Gibson G, Courtial J, Padgett M, Vasnetsov M, Pas'ko V, Barnett S, Franke-Arnold S. Free-space information transfer using light beams carrying orbital angular momentum. Opt. Express 2004; 12(22): 5448-5456.

[63] Djordjevic IB, Arabaci M, Xu L, Wang T. Spatial-domain-based multidimensional modulation for multi-Tb/s serial optical transmission. Opt. Express 2011; 19(7): 6845-6857.

[64] Lerber TV, Honkanen S, Tervonen A, Ludvigsen H, Küppers F. Optical clock recovery methods: Review (Invited). Opt. Fiber Technol. 2009; 15(4): 363-372.

[65] Mulvad HCH, Tangdiongga E, Waardt H, Dorren HJS. 40 GHz clock recovery from 640 Gbit/s OTDM signal using SOA based phase comparator. Electron. Lett. 2008; 44(2): 146-147.

[66] Oxenløwe LK, Gómez-Agis F, Ware C, Kurimura S, Mulvad HCH, Galili M, Nakajima H, Ichikawa J, Erasme D, Clausen AT, Jeppesen P. 640-Gbit/s data transmission and clock recovery using an ultrafast periodically poled lithium niobate device. J. Lightwave Technol. 2009; 27(3): 205-213.

[67] Takara H, Ono H, Abe Y, Masuda H, Takenaga K, Matsuo S, Kubota H, Shibahara K, Kobayashi T, Miaymoto Y. 1000-km 7-core fiber transmission of 10X96-Gb/s PDM-16QAM using Raman amplification with 6.5 W per fiber. Opt. Express 2012; 20(9): 10100-10105.

[68] Liu X, Chandrasekhar S, Chen X, Winzer PJ, Pan Y, Taunay TF, Zhu B, Fishteyn M, Yan MF, Fini JM, Monberg EM, Dimarcello FV. 1.12-Tb/s 32-QAM-OFDM superchannel with 8.6-b/s/Hz intrachannel spectral efficiency and space-division multiplexed transmission with 60-b/s/Hz aggregate spectral efficiency. Opt. Express 2011; 19(26): B958-B964.

[69] Al Amin A, Li A, Chen S, Gao G, Shieh W. Dual-LP11 mode 4X4 MIMO-OFDM transmission over a two-mode fiber. Opt. Express 2011; 19(17): 16672-16679.

[70] Ryf R, Randel S, Gnauck AH, Bolle C, Sierra A, Mumtaz S, Esmaeelpour M, Burrows EC, Essiambre RJ, Winzer PJ, Peckham DW, McCurdy AH, Lingle R. Mode-division multiplexing over 96 km of few-mode fiber using coherent 6 × 6 MIMO processing. J. Lightwave Technol. 2012; 30(4): 521-531.

[71] Koizumi Y, Toyoda K, Yoshida M, Nakazawa M. 1024 QAM (60 Gbit/s) single-carrier coherent optical transmission over 150 km. Opt. Express 2012; 20(11): 12508-12514.